Microelectromechanical Systems for Nanomechanical Testing: Displacement- and Force-Controlled Tensile Testing

C. Li[1], G. Cheng[1], H. Wang[1], Y. Zhu[1,*]

[1] Department of Mechanical and Aerospace Engineering, North Carolina State University, Raleigh, North Carolina 27695, USA

E-mail: yong_zhu@ncsu.edu

Abstract:

Background: MEMS-based nanomechanical testing has received much interests. However, it remains challenging to perform displacement- and force-controlled nanomechanical tests (e.g., stress relaxation and creep). **Objective**: We report a MEMS-based device for displacement- and force-controlled tensile testing of 1D nanomaterials using feedback control. **Methods**: The device consists of an electrostatic actuator, a load cell, and two differential capacitive sensors. A specimen is mounted between a fixed anchor on one side and a displacement sensor on the other side. Using a multi-channel capacitive readout, both specimen displacement and force (thus strain and stress) can be measured from the readout simultaneously, without the need of imaging that is often used for displacement measurement. **Results**: With the feedback control, both displacement- and force-controlled tensile testing can be achieved. The capability of the device is demonstrated in three representative tests of metallic nanowires – stress relaxation test, tensile test capturing rapid stress drop, and creep test. **Conclusions**: The reported MEMS device can be used for a range of tests where imaging for displacement measurement is not feasible, such as *ex-situ* tests and fatigue tests in different environments.

Keywords:

MEMS; nanomechanics; feedback control; stress relaxation; creep

1. Introduction

Nanomaterials exhibit outstanding mechanical properties such as ultrahigh strength [1, 2] superplasticity [3, 4], recoverable plasticity [5, 6], and large anelasticity and energy dissipation [7]. As such they have been used in a host of applications such as flexible and stretchable electronics, energy harvesting and storage, and nanoelectromechanical systems (NEMS) [8–10]. In addition, nanomaterials provide an ideal model system to probe some long-standing mechanics problems due to their small size (convenient for high-resolution in-situ testing) and well-defined microstructures. For example, metallic nanowires have bene used to investigate hydrogen embrittlement [11]; twinned nanowires have been used to explore dislocation-twin boundary interactions [12, 13];and Si nanowires have been used to study brittle-to-ductile transition [13]. In this paper, the focus will be placed on one-dimensional (1D) nanomaterials, while the results can be applicable to two-dimensional (2D) nanomaterials.

Over the past decades, a variety of testing methods have been devised to characterize mechanical properties of 1D nanomaterials, such as resonance in scanning or transmission electron microscopes (SEM or TEM), bending by atomic force microscope (AFM), contact resonance by AFM, and nanoindentation [14, 15]. In particular, microelectromechanical system (MEMS) based methods have received much interests [16–23]. MEMS offer a number of merits for nanomechanical testing including controlled actuation, high-resolution force/displacement measurements, and tiny size for *in-situ* SEM/TEM testing. More recently, MEMS-based methods have been explored for advanced nanomechanical testing, such as temperature-controlled testing [4], high-strain-rate testing [18, 24, 25], fatigue testing [26, 27],

and multiphysics testing (e.g., strain effect on electric resistance [28, 29]).

To probe dislocation mechanisms, it is of important relevance to conduct transient mechanical tests such as strain-rate jump, stress relaxation and creep[30]. The transient tests are also important for studying viscoelasticity. However, conducting such tests on nanomaterials is challenging. Qin et al. [5] reported an unusual time-dependent deformation behavior of penta-twinned Ag nanowires, where the nanowires undergo stress relaxation upon loading and complete plastic strain recovery upon unloading. The observed phenomenon is interesting, however, during stress relaxation not only did the stress drop, but also the strain increased. In another case, single-crystalline metallic nanowires were found to exhibit superplasticity as a result of continuous twin propagation [3, 4]. The superplasticity was preceded by a rapid stress drop associated with dislocation nucleation, which was accompanied by a rapid strain increase. However, details of the process were not captured.

The two examples above reveal an inadequacy of current MEMS-based testing devices, that is, the tensile testing device is neither displacement- nor force-controlled, which is necessary for capturing mechanical behaviors like stress relaxation, rapid stress drop due to certain relaxation mechanisms (e.g., dislocation or crack nucleation/propagation), creep and etc. This limitation originates from the limited stiffness of the load sensor (often comparable to or even smaller than that of the specimen); the load sensor deforms substantially in order to detect the force, so the specimen deformation is coupled with the load sensor deformation [18, 31, 32]. Furthermore, in the case of rapid stress drop, release of the stored elastic energy in the load sensor could trigger premature failure of the specimen, as evidenced in frequently observed brittle-like behavior in metallic nanowires [2].

To address this issue, a straightforward method is to increase the stiffness of the load sensor. It did prevent catastrophic fracture in nanowires, leading to the observation of stable plasticity. However, the drawback is that the force cannot be measured [33]. Another method, somewhat surprising, is to use a very compliant load sensor, at least for creep tests. This way the load drop due to the specimen elongation (and simultaneously the load sensor retraction) was reduced substantially. Subsequently a laborious manual feedback process was employed to reposition the load sensor and maintain the constant force [34]. The third method is to employ electronic feedback control. Pantano et al. [35] developed a feedback control scheme by adding an additional actuator at the far end of the capacitive load sensor, which can pull the load sensor back to the initial position based on the capacitance signal via feedback control. Using this scheme displacement-controlled loading was realized. The force cannot be directly obtained using the load sensor; rather it is obtained by the feedback voltage applied to the additional actuator. One limitation is that an extra actuator must be added. In addition, this scheme cannot realize force-controlled loading. In addition to capacitance, other mechanisms have been explored for feedback control such as piezoresistivity [36].

In this paper, we report a MEMS-based nanomechanical testing device using a new electronic feedback control scheme that can achieve both displacement- and force-controlled tensile testing without the need for an additional actuator. The device is comprised of an electrostatic actuator and two capacitive sensors. Feedback control is implemented using a proportional–integral–derivative (PID) controller directly on the electrostatic actuator. Both elongation and force of the specimen can be obtained digitally in real time. The rest of the paper starts with device overview and calibration, followed with implementation of the

feedback loop. In the end, we demonstrate the capability of the device in three representative tests of metallic nanowires – stress relaxation test, tensile test capturing rapid stress drop, and creep test.

2. Device Overview

Fig. 1(a) and (b) show the SEM image and corresponding schematic of the MEMS device, respectively. The device consists of an electrostatic (comb-drive) actuator, two interdigitated capacitive sensors, a load cell, and a gap for specimen mounting [37]. The shuttle is supported by four beams. Fig. 1(c) shows the lumped mechanical model of the device. When a specimen is mounted across the specimen gap, the load cell and the specimen can be considered as two springs connecting in series, taking the same force. Sensor B can be used to measure the elongation of specimen. Sensors A and B combined can be used to measure the elongation of the load cell, from which the force on the specimen (equal to that on the load cell) can be calculated, given the load cell stiffness. The device was fabricated using the MEMSCAP SOI-MUMPs process where the silicon structural layer thickness was chosen to be 25 μm.

Of note is the device configuration used here, which is different from most MEMS-based nanomechanical testing devices where a specimen is placed between the actuator and the load sensor [19, 32]. A unique advantage of this device is that it enables using one capacitive readout to record both capacitive sensors simultaneously. Most of the MEMS testing devices have only one capacitive sensor for load measurement, while the displacement is measured by other means such as SEM or optical imaging [19, 32]. Two capacitive sensors have been

introduced. However, two separate capacitive readouts have to be used, one for each sensor, which requires that the two sensors be electrically isolated using insulators (e.g., epoxy [38]). This obviously increases the fabrication complexity and might cause additional compliance issue. For our device configuration, there is no need of electric isolation between the two capacitive sensors. More details on the capacitive readout are provided in Section 3.2. Another advantage of our device configuration is elimination of the specimen rigid body motion due to the load sensor displacement as in most MEMS devices, which makes tracking the specimen deformation easier during *in-situ* testing.

2.1. Comb-drive Actuator

Comb-drive electrostatic actuator is used for actuation. Compared to other types of actuators such as electrothermal actuator and parallel-plate electrostatic actuator, comb-drive actuator can provide a nearly constant force and no heating effect. The actuation force is given by [19, 32]

$$F_A = N\varepsilon(\frac{t}{d})V^2 \quad (1)$$

where N is the number of pairs of comb fingers, ε is the permittivity, t is the thickness of the structure (=25 μm), d is the lateral gap between comb fingers (nominal value: 2 μm), and V is the applied voltage. For the device reported in this paper, N = 1056, providing an actuation force of 105 μN under an applied voltage V of 30 volt. Actual dimensions were measured from SEM images of the device after fabrication.

2.2. Capacitive Sensors

The displacement sensors A and B are differential capacitive sensors, which can provide a quasi-linear relationship between displacement and capacitance change [39],

$$\Delta C = 2N\varepsilon Ax(\frac{1}{d-x} - \frac{1}{d+x}) \quad (2)$$

where N is the number of sensor units (=16), A is the overlapping area of two adjacent plates (nominal value: 6750 μm^2), d is the initial gap between the adjacent plates (nominal value: 2 μm), and x is the displacement. Considering that x is much smaller than d, Eq. (2) simplifies as quasilinear relationship,

$$\Delta C \approx 2N\varepsilon A\frac{x}{d^2} \quad (3)$$

Theoretical sensitivity of present device for both sensors A and B was estimated to be around 0.4 fF/nm.

2.3. Load Cell

In order to test nanomaterials of different strengths, o-shaped load cells with different dimensions were designed. The o-shaped load cell consists of four clamped-guided beams whose stiffness can be calculated using a simple beam theory considering that the beam deflection is an insignificant fraction of the beam length.

$$k_{LC} = \frac{Ew^3t}{L^3} \quad (4)$$

where E is the Young's modulus of Si, and w and L are the width and length of the clamped-guided beams, respectively. Finite element analysis (FEA), based on the measured dimensions and the calibrated material constants, was used to verify the stiffness of the load cell. The devices used here were fabricated using the SOI-MUMPs process. In this case, the material constants were obtained previously from an atomic force microscopy (AFM) cantilever-based calibration [36]. Also in the silicon-on-insulator (SOI) process, the device (Si) layer is preexisting without going through the high-temperature deposition process.

Hence the residual stress in the device layer was neglected in the FEA. Other methods to calibrate the material constants include resonance of the device [39].

3. Results and Discussion

3.1. Calibration of the Actuator

To calibrate the comb drive actuator, a DC voltage was applied between the stationary electrode and the movable electrode (i.e. the shuttle) of the actuator. The DC voltage increased in a step of 2 V, and the corresponding displacement was measured from SEM imaging of the specimen gap area, see Fig. 2(a) and (b). Fig. 2 (c) plots the displacement as a function of the actuation voltage showing a quadratic relationship, as expected from Eq. (1). When no specimen mounted, the theoretical displacement of the shuttle can be calculated following

$$x = \frac{F_A}{k_{SB}} \tag{5}$$

where F_A is the actuation force calculated using Eq. (1), and k_{SB} is the stiffness of the four supporting beams. k_{SB} was also verified by FEA. The analytical result is in good agreement with the experimental one, as shown in Fig. 2(c).

3.2. Calibration of Capacitive Sensors

A commercially available differential capacitive readout (AT1006, ACT-LSI)[37] was used to measure the capacitance differences (ΔC) in both capacitive sensors A and B simultaneously. The readout was designed for capacitive three-axis accelerometer; hence it can connect to up to three differential capacitive sensors. The readout converts the capacitance signal of each sensor into a voltage signal through the corresponding channel. In this work, two channels (X and Y) were used, connecting to sensors A and B, respectively.

Hence, both force and elongation of a specimen can be measured using the readout, which enables the MEMS device to be used for *ex-situ* tests or time-consuming tests such as fatigue test and stress relaxation in different environments. Of note is that another type of commercially available differential capacitive readout (MS3110, Microsensors) has been widely used for MEMS-based nanomechanical testing [38, 39]. However, one MS3110 readout can only connect to one differential capacitive sensor. Two readouts (and hence the two capacitive sensors), if used together, must be electrically isolated [38].

Fig. 3 shows the functional block diagram of the readout and connection to the MEMS testing device. The core of AT1006 is a capacitance to voltage (C/V) converter (i.e., an op amp integrator with periodically on-off switch across the feedback capacitor C_{FB}). Three channels share the C/V converter in a time division manner, which is achieved by applying shifted periodic modulated pulses to the sensors. The converted voltage is held in a sample-and-hold circuit in synchronization with the applied pulse for each channel. The gain (or sensitivity, the highest of 150 V/pF) and offset can be trimmed through registers inside and the data can be stored in an on-chip EEPROM. Here a relatively low sensitivity of the readout, 18 V/pF, was selected considering the maximum output voltage cannot exceed 5 V.

To calibrate the capacitive sensor, an actuation voltage was applied to the comb drive actuator in a step of 2 V again, which caused displacements in capacitive sensors A and B. In every step, the output voltages for both channels, connecting to sensors A and B, were measured. The capacitance changes were then calculated and plotted against the displacement that was measured in SEM (Quanta 3D FEG dual beam with spatial resolution of 1.2 nm), as shown in Fig. 4. The capacitance change shows a linear relationship with the displacement,

which agrees well with the analytical result using Eq. (2).

3.3. Implementation of feedback control

As mentioned earlier, an advantage of our device configuration is that elongation of the specimen is equal to the displacement of sensor B, which can be measured by the capacitive readout AT1006. Using this measured displacement as the process variable, a feedback loop can be implemented to control the elongation of specimen using a DAQ (NI-USB 6009) and a Labview program. Fig. 5(a) shows the block diagram of the feedback loop. Output voltage of AT1006 is first sampled by the DAQ, the Labview program converts the voltage signal to displacement using the calibration results and compare it with the set (desired) displacement, the error is then fed to a PID controller, and finally an output voltage is generated through the DAQ that is further amplified to serve as the actuation voltage.

Other than the displacement control (i.e., maintaining a constant displacement of sensor B), the current device configuration is also suitable for force control since the force on the specimen can be easily calculated if displacements of both sensors A and B are known. A similar feedback loop for force control is shown in Fig. 5(b), where the only difference from the displacement control is an extra step (i.e., force calculation) after acquiring the displacements of the two sensors.

The performance of the feedback control was examined in terms of speed and accuracy. To evaluate control speed, step response for an input of 50 nm displacement (sensor B) was studied where a PI controller with the proportional and integral parameters tuned by the Ziegler-Nichols method was used [40]. As can be seen from Fig. 6(a), the rising time was about 15 ms while the settling time was 60 ms. Note that there was about 6 ms delay time,

which is because the maximum update rate of analog output for the DAQ we used, NI-USB 6009, is 150 Hz. To evaluate control accuracy, the displacement setpoint was hold at 20, 40 and 60 nm for about 3 minutes, during which 20 SEM images were taken; displacements were extracted from the images subsequently. Fig. 6 shows the displacement setpoints together with the measured displacements during the holding periods. It can be seen that the measured displacements are about 1 nm in error from the setpoint, which is much better than previously reported (~20 nm) [35].

3.4. Applications in Nanomechanical Testing

In order to demonstrate the feedback control capabilities, three types of tests were carried out inside SEM (FEI Quanta 3D FEG) – stress relaxation test, tensile test capturing rapid stress drop, and creep test. For all these tests, metallic nanowires were picked up from sources using a nanomanipulator (Klocke Nanotechnik, Germany) and clamped on the MEMS device using e-beam induced deposition of Pt [31]. Both force and elongation of the specimens were obtained from the capacitive readout following the method aforementioned. Given the diameters and gauge lengths of the specimens (measured from SEM images before testing), stress and strain were calculated assuming a circular cross section. Of note is that all the nanowires tested in this work were bottom-up synthesized with high quality (e.g., being straight and uniform in diameter). Using nanomanipulation, the nanowire specimens were well aligned with the loading axis (i.e., misalignment within $\pm 1^{o}$).

To demonstrate the device capability for displacement-controlled testing, penta-twinned Ag nanowires were selected. The penta-twinned Ag nanowires were synthesized by the

polyol method [41, 42], with a <110> axial orientation. As mentioned in the introduction, it has been found from both experiments and atomistic simulations that penta-twinned Ag nanowires exhibit stress relaxation as a result of vacancy diffusion assisted dislocation nucleation [5]. In the previous work, the MEMS device used was not capable of displacement control. An otherwise identical experiment except under displacement control was conducted here with the current MEMS device, aiming for a true stress relaxation test. After the Ag nanowire was mounted, displacement setpoint for the feedback loop was increased gradually to 40 nm (1.48% strain, given the gauge length of 2.7 μm), and then was maintained at that value for 10 minutes. Fig. 7(a) shows the stress-strain curve of the specimen tested, with the corresponding strain versus time and stress versus time relationships shown in Fig. 7(b) and (c), respectively. It can be seen that the stress relaxed during the holding period while the strain remained constant, which indicates the capability of this MEMS device for true stress relaxation testing.

Another demonstration of displacement-controlled testing came from tensile testing of an Au nanowire. The Au nanowires are single crystalline with a <110> axial orientation, synthesized via physical vapor deposition under molecular beam epitaxy conditions [43]. In this case, the displacement was set to linearly increase with time during the tensile test until fracture of the nanowire. Fig. 8 shows the testing results for this experiment. As can be seen in Fig. 8(a), the stress initially increased linearly with strain until strain reached 1.75%, which is the proportionality limit. Young's modulus of 93.5 GPa was measured, higher than the value of bulk Au. This might be due to two reasons: 1) elasticity size effect that has been reported for metallic nanowires [41, 44], or 2) underestimating the nanowire cross-sectional

area by assuming the circular cross section. Of note is that bottom-up synthesized nanowires typically have a polygonal cross section with well-developed facets (e.g., pentagon for penta-twinned Ag nanowires [45] and truncated rhomb or hexagon for single-crystalline Ag nanowires [4]). After 1.75% strain, the stress-strain curve showed a tendency of levelling off, indicating the emergence of plastic deformation. At 2.15% strain, a drastic stress drop was captured, following which the stress increased again until fracture. The stress drop is attributed to rapid nucleation and propagation of multiple leading partial dislocations from the surface as predicted by atomistic simulations [5, 46]. From Fig. 8(b) and (c), it can be seen that when the stress drop occurred, the displacement (or strain) remained constant according to the displacement setpoint, which indicates the capability of this MEMS device for capturing rapid stress drop due to dislocation nucleation and propagation.

To demonstrate the device capability for force-controlled testing, a creep test was carried out where the force was maintained constant after loading the specimen to a certain stress level. Penta-twinned Ag nanowires were used again. The stress-strain curve, strain-time curve, and stress-time curve are shown in Fig. 9 (a), (b) and (c), respectively. It can be seen that during the holding period the strain gradually increased while the stress remained constant, which indicates the capability of this MEMS device for true creep testing.

Of note is that in all three tests, the relative noise floor of stress is larger than the strain counterpart. This can be attributed to the fact that the force is calculated based on the difference in displacements of sensors A and B. Hence, the relative noise floor of stress should be twice that of strain, which can be seen in Figs. 7-9.

As mentioned in the Introduction, stress relaxation and creep are commonly used methods

to probe dislocation mechanisms. Dislocation activities including nucleation, motion and interaction with other defects are thermally activated. Activation parameters include activation energy and activation volume. The apparent activation volume can be obtained by fitting the stress relaxation and creep data. In the stress relaxation test, the stress decrease as a function of time can be fitted as

$$\Delta\sigma = -\frac{kT}{V_r}\ln(1 + t / c_r) \tag{6}$$

where $\Delta\sigma$ is the amount of stress decrease, V_r is the apparent activation volume of stress relaxation, c_r is the time constant, k is the Boltzmann constant, T is the temperature, t is the test time.

Similarly, In the creep test, the strain increase as a function of time can be fitted as

$$\Delta\gamma_p = \frac{kT}{MV_c}\ln(1 + t / c_c) \tag{7}$$

where $\Delta\gamma_p$ is the increased plastic strain, M is the Young's modulus of the specimen, V_c is the apparent activation volume of creep, and c_c is the time constant. Note that in Eq. (6) or (7), resolved shear stress or strain should be used.

To fit the stress relaxation and creep data, nonlinear regression using Eqs. (6) and (7) was applied. The Levenberg-Marquardt nonlinear least square algorithm was used with a maximum iteration number of 600 and termination of 10^{-6} for the residual sum of square. The apparent activation volumes are obtained as $5.70b^3$ and $2.51b^3$, respectively, from the stress relaxation and creep tests, where b denotes the magnitude of the Burgers vector.

The activation volume can serve as an effective kinetic signature of the rate-controlling deformation mechanism. This is because different rate-limiting processes can have drastically

different characteristic activation volumes, e.g., ~0.1b^3 for lattice diffusion, ~1–10b^3 for surface dislocation nucleation, and ~100–1000b^3 for Orowan looping through forest dislocation intersections. It is now well known that surface dislocation nucleation is the dislocation mechanism for single-crystalline nanowires [47, 48]. Molecular dynamics simulations previously showed surface dislocation nucleation occurs during the stress relaxation of penta-twinned Ag nanowires [5]. However, the obtained activation volumes in this work are relatively large compared to that for surface dislocation nucleation, indicating that there might exist other dislocation mechanisms in addition to surface dislocation nucleation. The apparent activation volume was measured to be about 20b^3 in nanotwinned Cu, which was attributed to twin-boundary-mediated cross-slip of dislocations [49]. It is likely that dislocation-twin boundary interaction [50] contributes to the measured activation volumes in penta-twinned Ag nanowires. Of note is that the activation volume from the stress relaxation test is smaller than that from the creep test. This is because the stress level during the stress relaxation test is higher than that during the creep test. It has been shown that activation volume is stress dependent, decreasing with increasing stress.

4. Conclusions

In summary, we reported a MEMS device for tensile testing of nanomaterials, which consists of an electrostatic actuator and two capacitive displacement sensors with a load cell in between. The unique advantage of this device is that both specimen displacement and force can be measured simultaneously using one capacitive readout. As a result, both displacement- and force-controlled testing can be achieved based on feedback control using a PID controller.

Three representative tests, i.e., stress relaxation of penta-twinned Ag nanowires, tensile test of Au nanowires with rapid stress drop, and creep of penta-twinned Ag nanowires, were carried out to demonstrate the device capability of displacement- and force-controlled tensile testing of nanomaterials. The extracted activation volumes from the stress relaxation and creep tests indicate that additional dislocation mechanisms (e.g., dislocation-twin boundary interactions) exist in addition to surface dislocation nucleation in penta-twinned Ag nanowires, and that activation volume is stress dependent, decreasing with increasing stress. As both the force and displacement are measured digitally, the reported MEMS device can be extended to *ex-situ* tests and fatigue tests in different environments, where imaging for displacement measurement is not feasible.

5. Acknowledgement

The authors gratefully acknowledge financial support from the National Science Foundation (NSF) through Award Nos. CMMI-1762511 and 1929646. The authors would like to thank Dr. G. Richter for providing the Au nanowires.

Compliance with Ethical Standards

The authors declare no competing financial interest.

References:

1. Zhu T, Li J (2010) Ultra-strength materials. Prog. Mater. Sci. 55:710–757
2. Richter G, Hillerich K, Gianola DS, et al (2009) Ultrahigh strength single crystalline nanowhiskers grown by physical vapor deposition. Nano Lett 9:3048–3052. https://doi.org/10.1021/nl9015107
3. Seo JH, Yoo Y, Park NY, et al (2011) Superplastic deformation of defect-free Au nanowires via coherent twin propagation. Nano Lett 11:3499–3502. https://doi.org/10.1021/nl2022306
4. Yin S, Cheng G, Richter G, et al (2019) Transition of Deformation Mechanisms in Single-Crystalline Metallic Nanowires. ACS Nano 13:9082–9090. https://doi.org/10.1021/acsnano.9b03311
5. Qin Q, Yin S, Cheng G, et al (2015) Recoverable plasticity in penta-twinned metallic nanowires governed by dislocation nucleation and retraction. Nat Commun 6:5983. https://doi.org/10.1038/ncomms6983
6. Bernal RA, Aghaei A, Lee S, et al (2015) Intrinsic bauschinger effect and recoverable plasticity in pentatwinned silver nanowires tested in tension. Nano Lett 15:139–146. https://doi.org/10.1021/nl503237t
7. Cheng G, Miao C, Qin Q, et al (2015) Large anelasticity and associated energy dissipation in single-crystalline nanowires. Nat Nanotechnol 10:687–691. https://doi.org/10.1038/nnano.2015.135
8. Yao S, Zhu Y (2015) Nanomaterial-Enabled Stretchable Conductors: Strategies, Materials and Devices. Adv Mater 27:1480–1511. https://doi.org/10.1002/adma.201404446
9. Zhang Q, Uchaker E, Candelaria SL, Cao G (2013) Nanomaterials for energy conversion and storage. Chem Soc Rev 42:3127–3171. https://doi.org/10.1039/c3cs00009e
10. Loh OY, Espinosa HD (2012) Nanoelectromechanical contact switches. Nat Nanotechnol 7:283–295. https://doi.org/10.1038/nnano.2012.40
11. Yin S, Cheng G, Chang TH, et al (2019) Hydrogen embrittlement in metallic nanowires. Nat Commun 10:2004. https://doi.org/10.1038/s41467-019-10035-0
12. Wang J, Sansoz F, Huang J, et al (2013) Near-ideal theoretical strength in gold nanowires containing angstrom scale twins. Nat Commun 4:1742. https://doi.org/10.1038/ncomms2768
13. Cheng G, Yin S, Chang TH, et al (2017) Anomalous Tensile Detwinning in Twinned Nanowires. Phys Rev Lett 119:256101. https://doi.org/10.1103/PhysRevLett.119.256101
14. Zhu Y, Ke C, Espinosa HD (2007) Experimental techniques for the mechanical characterization of one-dimensional nanostructures. Exp. Mech. 47:7–24
15. Zhu Y (2017) Mechanics of Crystalline Nanowires: An Experimental Perspective. Appl. Mech. Rev. 69:010802
16. Zhu Y, Chang TH (2015) A review of microelectromechanical systems for nanoscale mechanical characterization. J. Micromechanics Microengineering 25:093001
17. Kang W, Rajagopalan J, Saif MTA (2010) In situ uniaxial mechanical testing of small

scale materials - A review. Nanosci. Nanotechnol. Lett. 2:282–287
18. Naraghi M, Chasiotis I, Kahn H, et al (2007) Novel method for mechanical characterization of polymeric nanofibers. Rev Sci Instrum 78:085018. https://doi.org/10.1063/1.2771092
19. Zhang D, Breguet JM, Clavel R, et al (2010) In situ electron microscopy mechanical testing of silicon nanowires using electrostatically actuated tensile stages. J Microelectromechanical Syst 19:663–674. https://doi.org/10.1109/JMEMS.2010.2044746
20. Naraghi M, Ozkan T, Chasiotis I, et al (2010) MEMS platform for on-chip nanomechanical experiments with strong and highly ductile nanofibers. J Micromechanics Microengineering 20:125022. https://doi.org/10.1088/0960-1317/20/12/125022
21. Kiuchi M, Matsui S, Isono Y (2007) Mechanical characteristics of FIB deposited carbon nanowires using an electrostatic actuated Nano Tensile testing device. J Microelectromechanical Syst 16:191–201. https://doi.org/10.1109/JMEMS.2006.889663
22. Lu Y, Ganesan Y, Lou J (2010) A Multi-step method for In situ mechanical characterization of 1-D nanostructures using a novel micromechanical device. Exp Mech 50:47–54. https://doi.org/10.1007/s11340-009-9222-0
23. Haque MA, Espinosa HD, Lee HJ (2010) MEMS for in situ testing - Handling, actuation, loading, and displacement measurements. MRS Bull 35:375–381. https://doi.org/10.1557/mrs2010.570
24. Ramachandramoorthy R, Gao W, Bernal R, Espinosa H (2016) High Strain Rate Tensile Testing of Silver Nanowires: Rate-Dependent Brittle-to-Ductile Transition. Nano Lett 16:255–263. https://doi.org/10.1021/acs.nanolett.5b03630
25. Li C, Zhang D, Cheng G, Zhu Y (2020) Microelectromechanical Systems for Nanomechanical Testing: Electrostatic Actuation and Capacitive Sensing for High-Strain-Rate Testing. Exp Mech 60:329–343. https://doi.org/10.1007/s11340-019-00565-5
26. Zhang H, Jiang C, Lu Y (2017) Low-Cycle Fatigue Testing of Ni Nanowires Based on a Micro-Mechanical Device. Exp Mech 57:495–500. https://doi.org/10.1007/s11340-016-0199-1
27. Baumert EK, Pierron ON (2013) Fatigue degradation properties of LIGA Ni films using kilohertz microresonators. J Microelectromechanical Syst 22:16–25. https://doi.org/10.1109/JMEMS.2012.2212422
28. Bernal RA, Filleter T, Connell JG, et al (2014) In Situ Electron Microscopy Four-Point Electromechanical Characterization of Freestanding Metallic and Semiconducting Nanowires. Small 10:725–733. https://doi.org/10.1002/smll.201300736
29. Zhang Y, Liu X, Ru C, et al (2011) Piezoresistivity characterization of synthetic silicon nanowires using a MEMS Device. J Microelectromechanical Syst 20:959–967. https://doi.org/10.1109/JMEMS.2011.2153825
30. Caillard D, Martin JL (2003) Thermally activated mechanisms in crystal plasticity. Elsevier
31. Zhu Y, Espinosa HD (2005) An electromechanical material testing system for in situ

electron microscopy and applications. Proc Natl Acad Sci U S A 102:14503–14508. https://doi.org/10.1073/pnas.0506544102
32. Espinosa HD, Zhu Y, Moldovan N (2007) Design and operation of a MEMS-based material testing system for nanomechanical characterization. J Microelectromechanical Syst 16:1219–1231. https://doi.org/10.1109/JMEMS.2007.905739
33. Shin J, Richter G, Gianola DS (2020) Suppressing instabilities in defect-scarce nanowires by controlling the energy release rate during incipient plasticity. Mater Des 189:108460. https://doi.org/10.1016/j.matdes.2019.108460
34. Naraghi M, Kolluru P V., Chasiotis I (2014) Time and strain rate dependent mechanical behavior of individual polymeric nanofibers. J Mech Phys Solids 62:257–275. https://doi.org/10.1016/j.jmps.2013.10.006
35. Pantano MF, Bernal RA, Pagnotta L, Espinosa HD (2015) Multiphysics design and implementation of a microsystem for displacement-controlled tensile testing of nanomaterials. Meccanica 50:549–560. https://doi.org/10.1007/s11012-014-9950-9
36. Ouyang J, Zhu Y (2012) Z-shaped MEMS thermal actuators: Piezoresistive self-sensing and preliminary results for feedback control. J Microelectromechanical Syst 21:596–604. https://doi.org/10.1109/JMEMS.2012.2189361
37. Tsuchiya T, Ura Y, Sugano K, Tabata O (2012) Electrostatic tensile testing device with nanonewton and nanometer resolution and its application to C 60 nanowire testing. J Microelectromechanical Syst 21:523–529. https://doi.org/10.1109/JMEMS.2011.2182503
38. Pant B, Choi S, Baumert EK, et al (2012) MEMS-Based Nanomechanics: Influence of MEMS Design on Test Temperature. Exp Mech 52:607–617. https://doi.org/10.1007/s11340-011-9526-8
39. Zhu Y, Moldovan N, Espinosa HD (2005) A microelectromechanical load sensor for in situ electron and x-ray microscopy tensile testing of nanostructures. Appl Phys Lett 86:013506. https://doi.org/10.1063/1.1844594
40. Åström KJ, Hägglund T (2004) Revisiting the Ziegler-Nichols step response method for PID control. J Process Control 14:635–650. https://doi.org/10.1016/j.jprocont.2004.01.002
41. Zhu Y, Qin Q, Xu F, et al (2012) Size effects on elasticity, yielding, and fracture of silver nanowires: In situ experiments. Phys Rev B - Condens Matter Mater Phys 85:045443. https://doi.org/10.1103/PhysRevB.85.045443
42. Wiley B, Sun Y, Xia Y (2007) Synthesis of Silver Nanostructures with Controlled Shapes and Properties. Acc Chem Res 40:1067–1076. https://doi.org/10.1021/ar7000974
43. Sedlmayr A, Bitzek E, Gianola DS, et al (2012) Existence of two twinning-mediated plastic deformation modes in Au nanowhiskers. Acta Mater 60:3985–3993. https://doi.org/10.1016/j.actamat.2012.03.018
44. Jing GY, Duan HL, Sun XM, et al (2006) Surface effects on elastic properties of silver nanowires: Contact atomic-force microscopy. Phys Rev B - Condens Matter Mater Phys 73:235409. https://doi.org/10.1103/PhysRevB.73.235409
45. Chang TH, Cheng G, Li C, Zhu Y (2016) On the size-dependent elasticity of penta-twinned silver nanowires. Extrem Mech Lett 8:177–183.

https://doi.org/10.1016/j.eml.2016.03.007
46. Park HS, Zimmerman JA (2005) Modeling inelasticity and failure in gold nanowires. Phys Rev B - Condens Matter Mater Phys 72:054106. https://doi.org/10.1103/PhysRevB.72.054106
47. Zhu T, Li J, Samanta A, et al (2008) Temperature and strain-rate dependence of surface dislocation nucleation. Phys Rev Lett 100:025502. https://doi.org/10.1103/PhysRevLett.100.025502
48. Zheng H, Cao A, Weinberger CR, et al (2010) Discrete plasticity in sub-10-nm-sized gold crystals. Nat Commun 1:144. https://doi.org/10.1038/ncomms1149
49. Lu L, Zhu T, Shen Y, et al (2009) Stress relaxation and the structure size-dependence of plastic deformation in nanotwinned copper. Acta Mater 57:5165–5173. https://doi.org/10.1016/j.actamat.2009.07.018
50. Narayanan S, Cheng G, Zeng Z, et al (2015) Strain Hardening and Size Effect in Five-fold Twinned Ag Nanowires. Nano Lett 15:4037–4044. https://doi.org/10.1021/acs.nanolett.5b01015

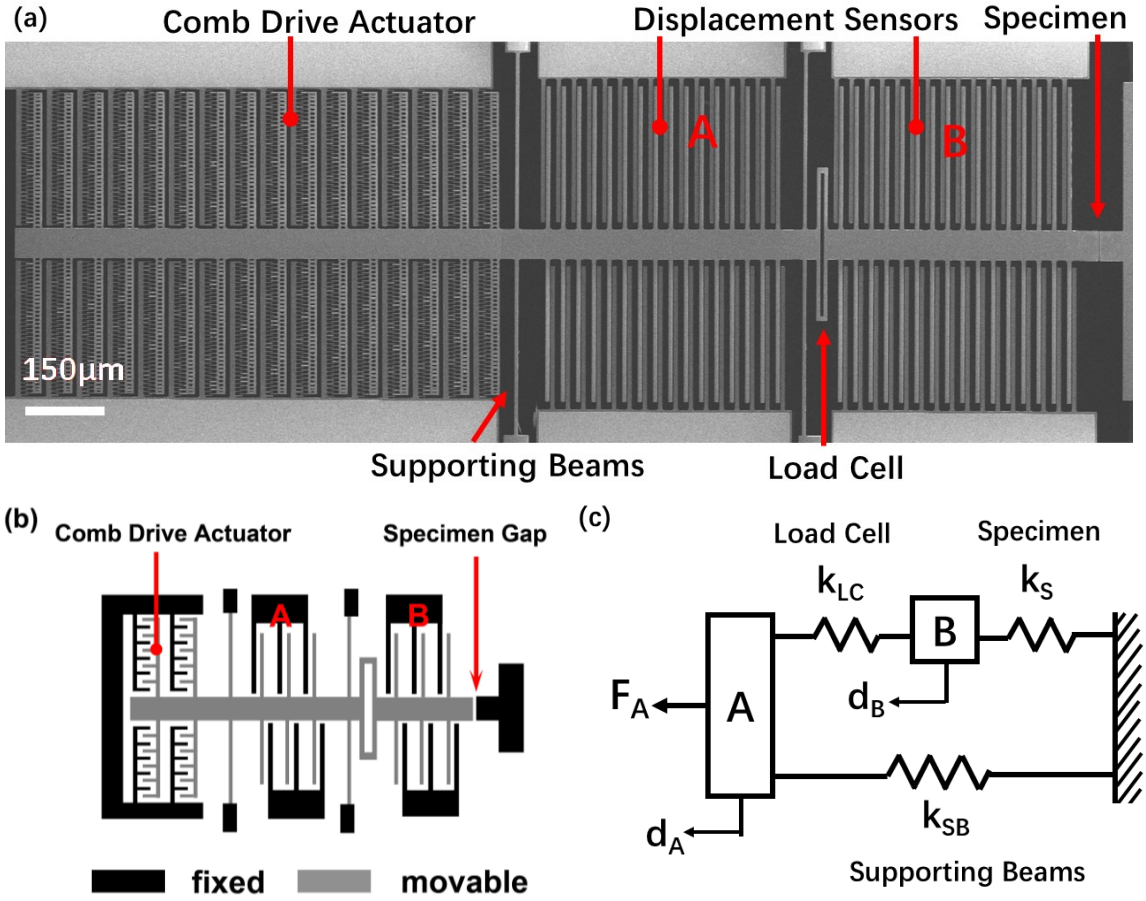

Fig. 1. (a) SEM micrograph of the fabricated MEMS device. (b) Schematic of the MEMS device configuration. (c) Lumped mechanical model of the device during tensile testing of a specimen.

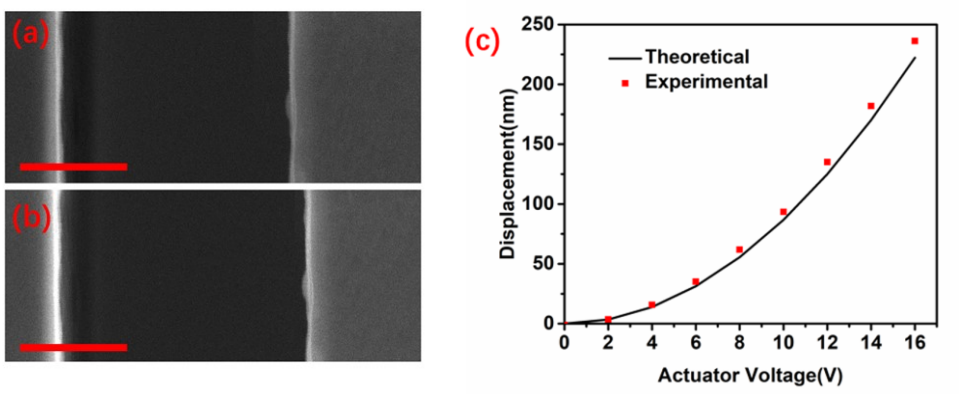

Fig. 2. Comb-drive actuator calibration results. Specimen gap when actuation voltage is (a) 0V and (b) 14V. Scale bar is 1um. (c) Displacement as a function of actuation voltage.

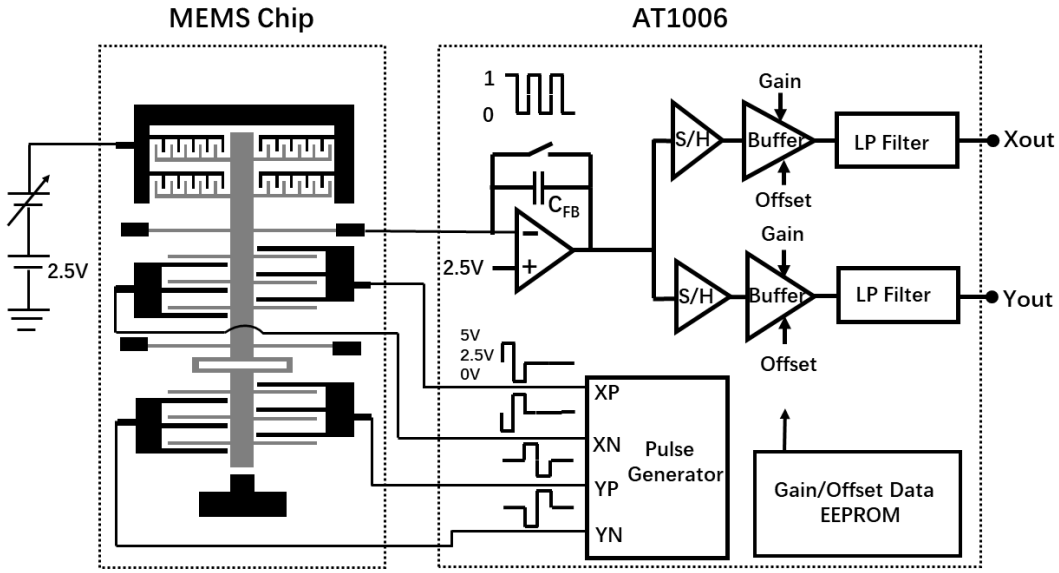

Fig. 3. Functional block diagram of capacitive readout AT1006 and its connection with the MEMS device.

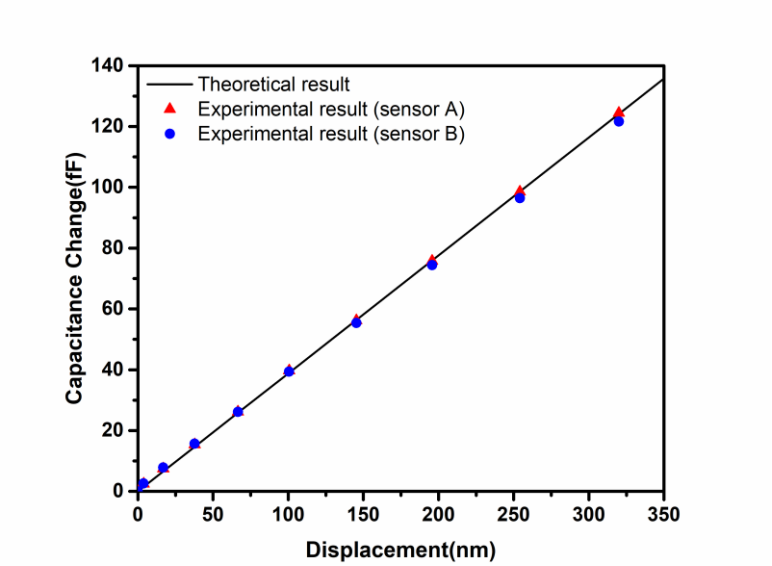

Fig. 4. Comparison of theoretical and experimental relationship between capacitance change and displacement for both displacement sensors.

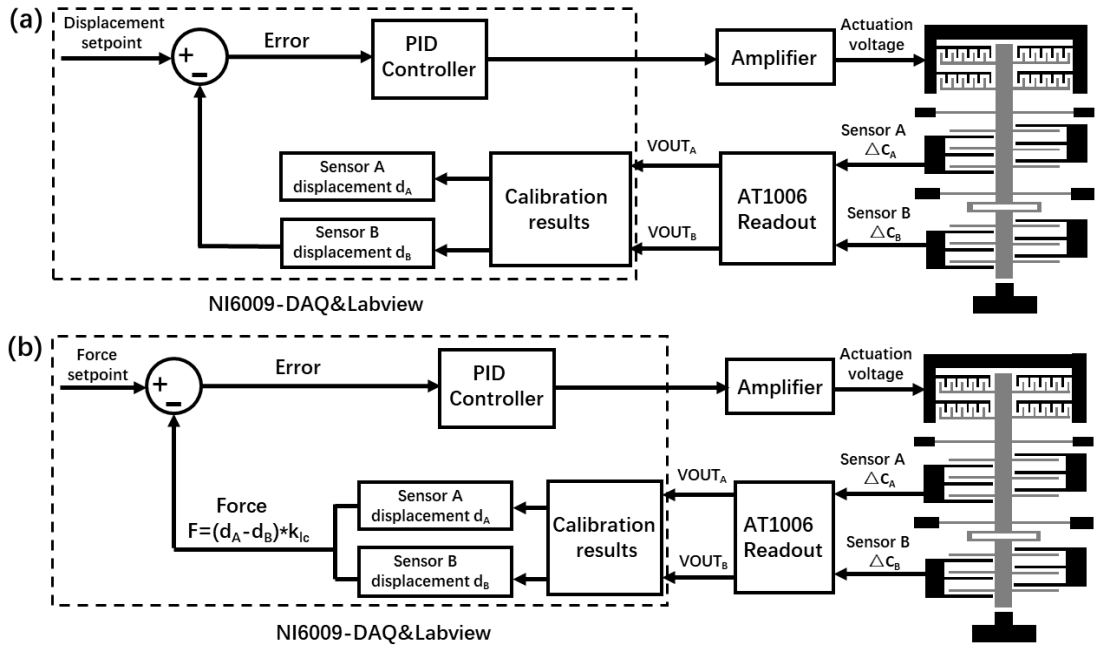

Fig. 5. Closed-loop block diagrams for (a) displacement control and (b) force control.

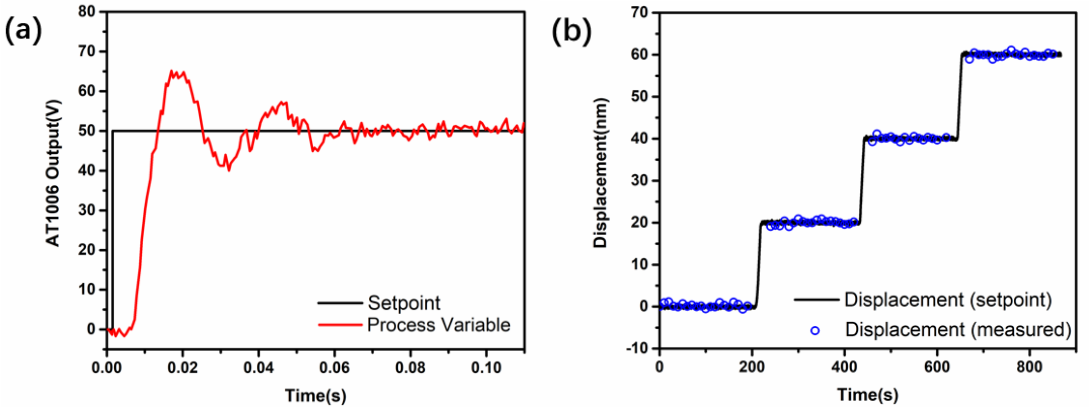

Fig. 6. Examination of performance of feedback control. (a) control speed. (b) control accuracy.

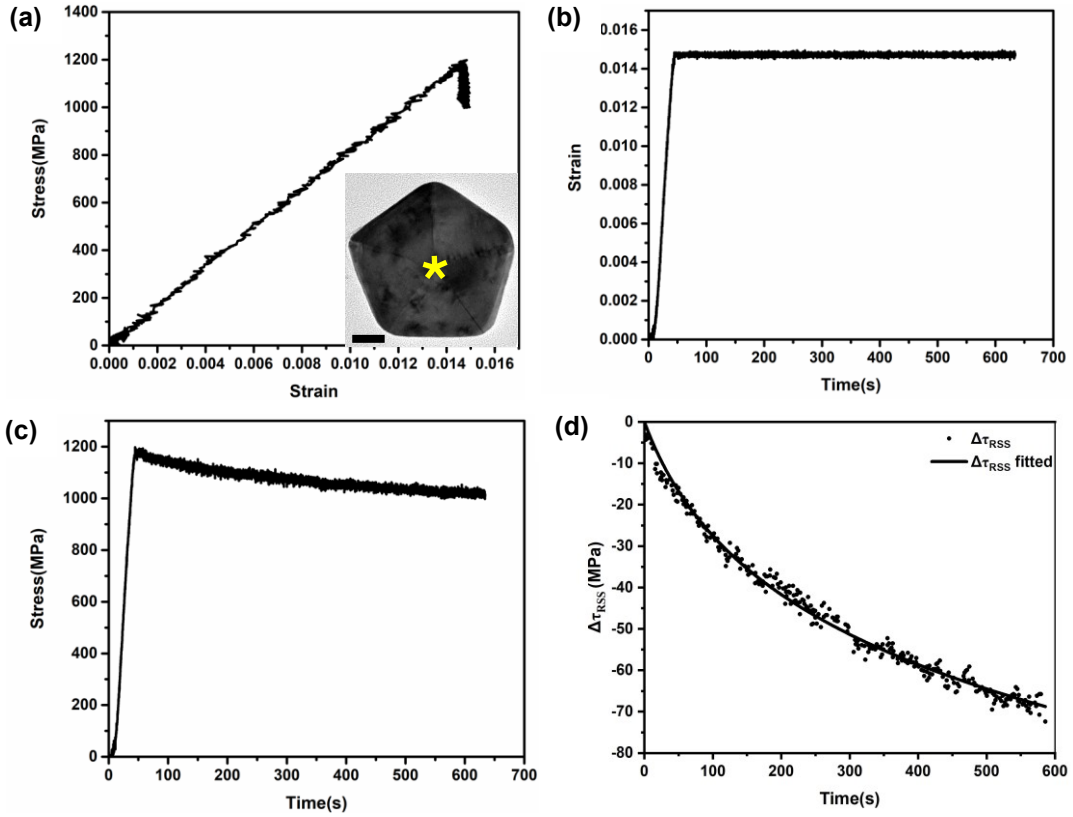

Fig. 7. Stress relaxation of a penta-twinned Ag nanowire. (a) Stress vs. strain. Insert is the cross-sectional TEM image of the tested NW, scale bar, 20 nm. (b) Strain vs. time. (c) Stress vs. time. (d) Experimental data and fitted curve of the shear stress decrease vs. time.

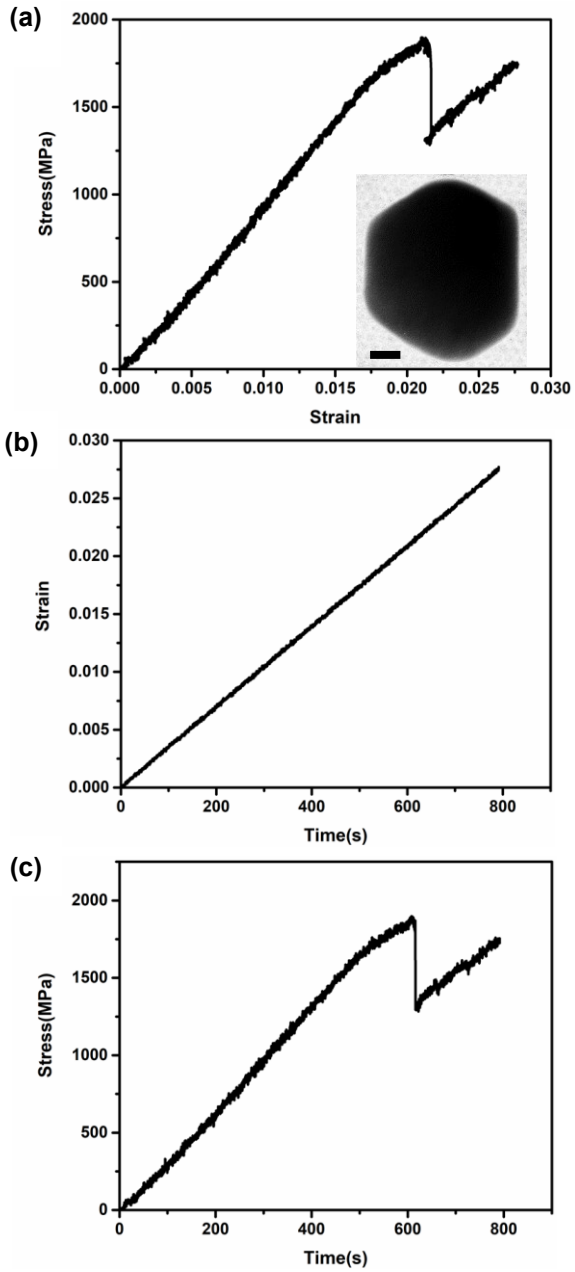

Fig. 8. Displacement-controlled tensile testing of a Au single-crystalline nanowire. (a) Stress-strain curve. Insert is the cross-sectional TEM image of the tested NW, scale bar, 20 nm. (b) Strain vs. time. (c) Stress vs. time.

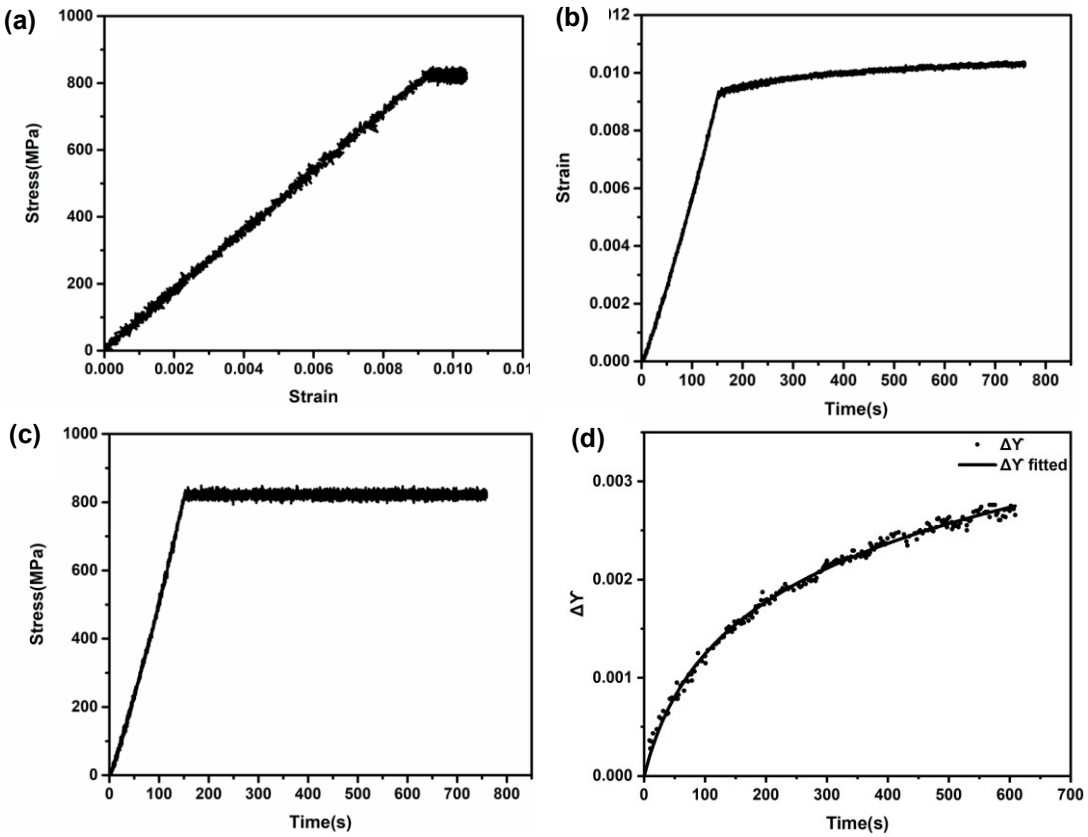

Fig. 9. Creep of a penta-twinned Ag nanowire. (a) Stress vs. strain. (b) Strain vs. time. (c) Stress vs. tme. (d) Experimental data and fitted curve of the shear strain increase vs. time.